# Chapter 12

# Pre-supernova evolution of massive stars

We have seen that low- and intermediate-mass stars (with masses up to $\approx 8\,M_\odot$) develop carbon-oxygen cores that become degenerate after central He burning. As a consequence the maximum core temperature reached in these stars is smaller than the temperature required for carbon fusion. During the latest stages of evolution on the AGB these stars undergo strong mass loss which removes the remaining envelope, so that their final remnants are C-O white dwarfs.

The evolution of *massive stars* is different in two important ways:

- They reach a sufficiently high temperature in their cores ($> 5{\times}10^8$ K) to undergo *non-degenerate carbon ignition* (see Fig. 12.1). This requires a certain minimum mass for the CO core after central He burning, which detailed evolution models put at $M_{\mathrm{CO-core}} > 1.06\,M_\odot$. Only stars with initial masses above a certain limit, often denoted as $M_{\mathrm{up}}$ in the literature, reach this critical core mass. The value of $M_{\mathrm{up}}$ is somewhat uncertain, mainly due to uncertainties related to mixing (e.g. convective overshooting), but is approximately $8\,M_\odot$.

  Stars with masses above the limit $M_{\mathrm{ec}} \approx 11\,M_\odot$ also ignite and burn fuels heavier than carbon until an Fe core is formed which collapses and causes a supernova explosion. We will explore the evolution of the cores of massive stars through carbon burning, up to the formation of an iron core, in the second part of this chapter.

- For masses $M \gtrsim 15\,M_\odot$, *mass loss by stellar winds* becomes important during all evolution phases, including the main sequence. For masses above $30\,M_\odot$ the mass-loss rates $\dot{M}$ are so large that the timescale for mass loss, $\tau_{\mathrm{ml}} = M/\dot{M}$, becomes smaller than the nuclear timescale $\tau_{\mathrm{nuc}}$. Therefore mass loss has a very significant effect on their evolution. The stellar wind mechanisms involved are in many cases not well understood, so that $\dot{M}$ is often quite uncertain. This introduces substantial uncertainties in massive star evolution. The effect of mass loss on massive star evolution is discussed in the first part of this chapter.

## 12.1 Stellar wind mass loss

Observations in the ultraviolet and infrared part of the spectrum show that luminous stars, with masses above about $15\,M_\odot$, undergo rapid mass outflows (stellar winds) that gradually erode their outer layers. An empirical formula that fits the average observed mass-loss rates of stars of roughly solar metallicity in the upper part of the HR diagram ($L \gtrsim 10^3\,L_\odot$) was derived by De Jager and others in 1988:

$$\log(-\dot{M}) \approx -8.16 + 1.77 \log\left(\frac{L}{L_\odot}\right) - 1.68 \log\left(\frac{T_{\mathrm{eff}}}{\mathrm{K}}\right) \qquad (\text{in } M_\odot/\mathrm{yr}). \tag{12.1}$$

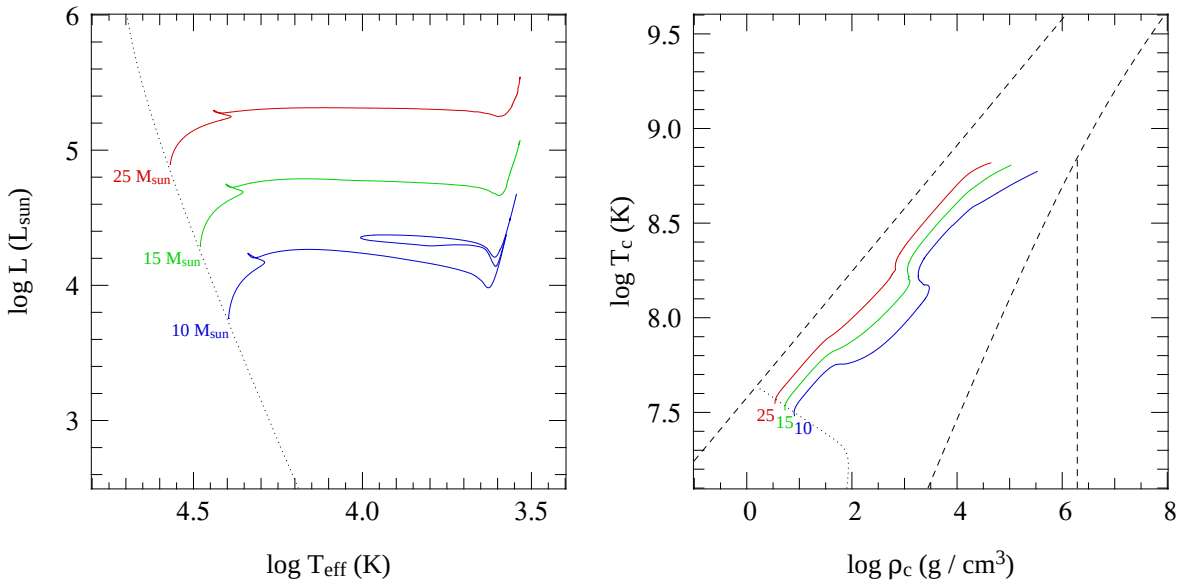


**Figure 12.1.** Evolution tracks in the HR diagram (left panel) and in the $\log \rho_c$-$\log T_c$ diagram (right panel) for stars with $Z = 0.02$ and $M = 10$, 15 and 25 $M_\odot$, computed with a moderate amount of overshooting. The tracks end when carbon is ignited in the centre, under non-degenerate conditions.

For example, for the 25 $M_\odot$ star depicted in Fig. 12.1 you can check by estimating $L$ and $T_{\rm eff}$ from the graph that this implies a mass loss of $5 \times 10^{-8}$ $M_\odot$/yr at the ZAMS, increasing up to $5 \times 10^{-7}$ $M_\odot$/yr at the end of the main sequence. By the end of the evolution track, when the star is a red supergiant, the mass-loss rate implied by the above formula has increased to $5 \times 10^{-5}$ $M_\odot$/yr.

The observed strong mass loss is probably caused by different mechanisms in different parts of the HR diagram.

### Radiation-driven stellar winds

Hot, luminous stars (OB-type main-sequence stars and *blue supergiants*, BSG) undergo a fast *radiation-driven stellar wind*. Radiation pressure at frequencies corresponding to absorption lines in the spectrum, where the interaction between photons and matter is strong, causes an outward acceleration. An upper limit to the mass-loss rate that can be driven by radiation is obtained by assuming that the photons transfer their entire momentum to the outflowing matter:

$$\dot{M} v_\infty < \frac{L}{c} \tag{12.2}$$

where $v_\infty$ is the terminal wind velocity at large distance from the star ('infinity'). A typical value of the terminal velocity is about three times the escape velocity, $v_\infty \approx 3 v_{\rm esc}$ (about 1000–3000 km/s for O-type stars). Comparing the mass-loss rates from eq. (12.1) with the upper limit shows that the empirical rates are indeed smaller, but only by a factor 1/3 to 1/6: apparently momentum is transferred quite efficiently from the photons to the wind. This can be attributed to the acceleration of the wind: the associated Doppler broadening of the spectral lines means a large part of the flux can be used (the outflowing atoms can absorb photons of a different, higher frequency as they get accelerated). This is a positive feedback mechanism that reinforces the wind driving.

The theory for radiation-driven winds is quite well developed, but the theoretical predictions for $\dot{M}$ are uncertain due to inhomogeneities in the wind ('clumping'). The uncertain clumping factor also affects the mass-loss rates inferred from observations, and current estimates are typically a factor

$\sim 3$ lower than the the empirical rate of eq. (12.1). Radiation-driven mass loss is also dependent on metallicity, because it is mostly the lines of the heavier elements that contribute to the line driving. A dependence $\dot{M} \propto Z^{0.7}$ has been inferred both theoretically and from observations.

**Red supergiant mass loss**

Cool, luminous stars known as *red supergiants* (RSG) undergo a slow but copious stellar wind that is probably driven by the same mechanism as the 'superwind' of AGB stars: a combination of stellar pulsations and radiation pressure on dust particles that form in the cool outer atmosphere. There are no theoretical predictions, so we must rely on observations which imply very high values of $\dot{M}$ up to $10^{-4} M_\odot$/yr (eq. 12.1).

Stars with $M \lesssim 40\,M_\odot$ spend a large fraction of their *core He-burning* phase as red supergiants. During this phase a large part or even the entire envelope can be evaporated by the wind, exposing the helium core of the star as a Wolf-Rayet (WR) star (see Sect. 12.1.2).

### 12.1.1 The Humphreys-Davidson limit and luminous blue variables

Observations of the most luminous stars in our Galaxy and in the Magellanic Clouds have revealed a clear upper limit to stellar luminosities that depends on the effective temperature (see Fig. 12.2). In particular there are no red supergiants in HR diagram with $\log(L/L_\odot) > 5.8$, which corresponds to the expected RSG luminosity of a star of $40\,M_\odot$. Apparently stars with $M \gtrsim 40\,M_\odot$ do not become red supergiants.

The upper limit in the HRD is known as the *Humphreys-Davidson limit* after its discoverers, Roberta Humphreys and Kris Davidson. At $T_{\rm eff}$ above 10 000 K the maximum luminosity increases gradually to $\log(L/L_\odot) = 6.8$ at 40 000 K (O stars).

The existence of the HD limit is interpreted as a (generalized) Eddington limit. We have seen in Sec. 5.4 that when the luminosity of a star exceeds the classical Eddington limit (eq. 5.38),

$$L_{\rm Edd} = \frac{4\pi c G M}{\kappa_{\rm e}}, \tag{12.3}$$

where $\kappa_{\rm e}$ is the electron-scattering opacity, the outward force due to radiation pressure on the free electrons exceeds the gravitational force (on the nuclei) inwards. The electrostatic coupling between

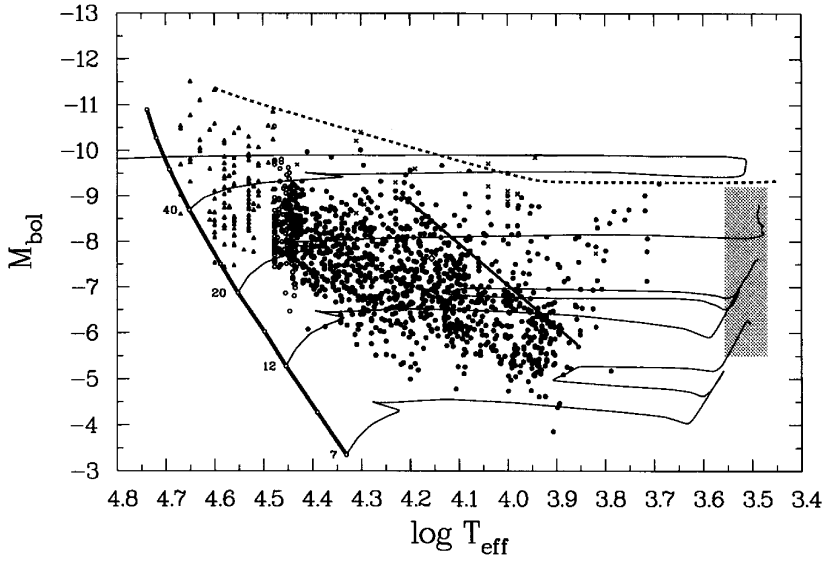


**Figure 12.2.** The HRD of the brightest supergiants in the LMC. The shaded region contains several hundred red supergiants that are not individually shown. The upper envelope of observed stars traced by the dotted line is known as the Humphreys-Davidson limit (the lower envelope is simply an observational cut-off). Figure adapted from Fitzpatrick & Garmany (1990, ApJ 363, 119).

electrons and ions means that the outer layers are accelerated outwards and the star becomes unstable. However, the *actual* opacity in the atmosphere is larger than the electron-scattering opacity, and decreases with temperature. Therefore the luminosity at which the radiation-pressure limit is reached is lower than the classical Eddington limit, and the decrease of the HD limit with decreasing $T_{\rm eff}$ can be explained at least qualitatively by this effect.

Luminous stars located near the HD limit are indeed observed to be very unstable, undergoing large excursions in the HRD and episodic mass loss with $\dot{M} \gtrsim 10^{-3}\,M_\odot$/yr during outbursts. These stars are known as *luminous blue variables* (LBVs), examples of which in our Galaxy are $\eta$ Carinae and P Cygni. The remnants of the vigorous mass loss episodes are seen as circumstellar nebulae, which in the extreme case of $\eta$ Car contains $\sim 10\,M_\odot$ ejected during an outburst in the mid-1800s. The nebula is considerably enriched in nitrogen, showing that the layers processed by CNO-cycling are being ejected. Stars losing mass due to LBV outbursts are destined to become *Wolf-Rayet stars*. The strong LBV mass loss prevents them from ever becoming red supergiants.

### 12.1.2 Wolf-Rayet stars

Wolf-Rayet (WR) stars are hot, very luminous stars with bright emission lines in their spectra. The emission indicates very strong, optically thick stellar winds, with mass-loss rates of $\dot{M} \sim 10^{-5} - 10^{-4}\,M_\odot$/yr. They are often surrounded by circumstellar nebulae of ejected material. The winds are probably driven by radiation pressure as for O stars, but multiple photon scattering in the optically thick outflow can increase the mass-loss rate to well above the single-scattering limit (eq. 12.2).

The spectra of WR stars reveal increased CNO abundances, indicating that they are the exposed H- or He-burning cores of massive stars. On the basis of the surface abundances they are classified into several subtypes:

**WNL stars** have hydrogen present on their surfaces (with $X_{\rm H} < 0.4$) and increased He and N abundances, consistent with equilibrium values from the CNO-cycle

**WNE stars** are similar to WNL stars in terms of their He and N abundances, but they lack hydrogen ($X_{\rm H} = 0$)

**WC stars** have no hydrogen, little or no N, and increased He, C and O abundances (consistent with partial He-burning)

**WO stars** are similar to WC stars with strongly increased O abundances (as expected for nearly complete He burning)

This is interpreted as an *evolutionary sequence* of exposure of deeper and deeper layers, as a massive star is peeled off to a larger and larger extent by mass loss (see Sec. 12.2).

## 12.2 Evolution of massive stars with mass loss in the HR diagram

Fig. 12.3 shows evolution tracks in the HRD for massive stars calculated with mass loss at metallicity $Z = 0.02$. As revealed by this figure, the evolutionary journey of a massive star through the HRD can be rather complicated. Evolution proceeds at nearly constant luminosity, because massive stars do not develop degenerate cores and most of the mass is in radiative equilibrium. However, the evolution track shows several left-right excursions and loops which depend on the mass of the star. The relation between the theoretical evolution tracks and the zoo of observed types of massive star encountered in Sec. 12.1 is described by the following *evolution scenario*, originally proposed by Peter Conti:

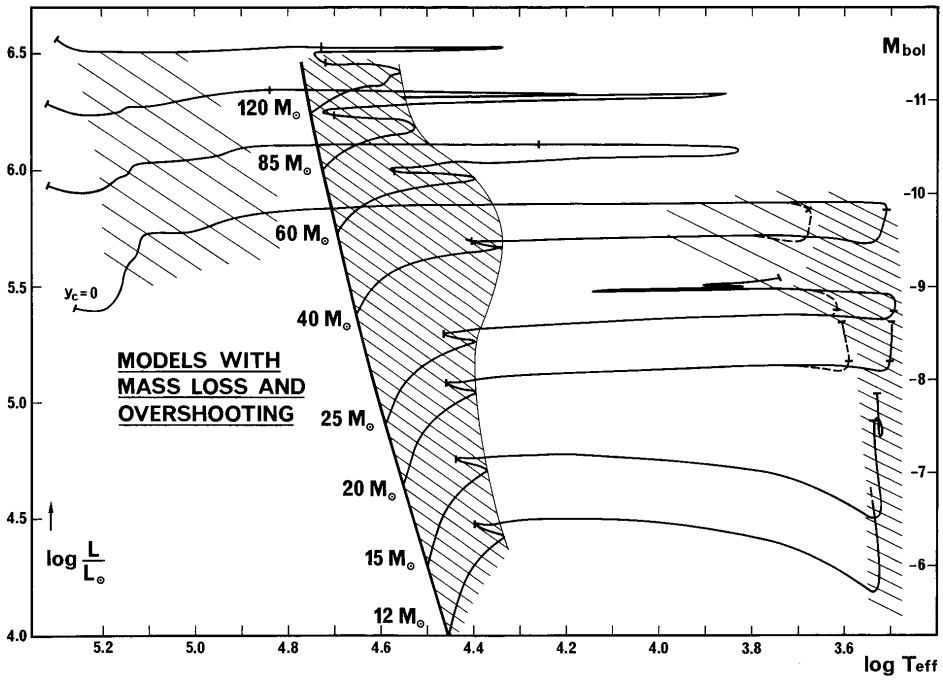


**Figure 12.3.** Evolution tracks of massive stars ($12 - 120\,M_\odot$) calculated with mass loss and a moderate amount of convective overshooting ($0.25\,H_P$). The shaded regions correspond to long-lived evolution phases on the main sequence, and during core He burning as a RSG (at $\log T_{\rm eff} < 4.0$) or as a WR star (at $\log T_{\rm eff} > 4.8$). Stars with initial mass $M > 40\,M_\odot$ are assumed to lose their entire envelope due to LBV episodes and never become RSGs. Figure from Maeder & Meynet (1987, A&A 182, 243).

| | |
|---|---|
| $M \lesssim 15\,M_\odot$ | MS (OB) → RSG (→ BSG in blue loop? → RSG) → SN II<br>mass loss is relatively unimportant, $\lesssim$ few $M_\odot$ is lost during entire evolution |
| $15\,M_\odot \lesssim M \lesssim 25\,M_\odot$ | MS (O) → BSG → RSG → SN II<br>mass loss is strong during the RSG phase, but not strong enough to remove the whole H-rich envelope |
| $25\,M_\odot \lesssim M \lesssim 40\,M_\odot$ | MS (O) → BSG → RSG → WNL → WNE → WC → SN Ib<br>the H-rich envelope is removed during the RSG stage, turning the star into a WR star |
| $M \gtrsim 40\,M_\odot$ | MS (O) → BSG → LBV → WNL → WNE → WC → SN Ib/c<br>an LBV phase blows off the envelope before the RSG can be reached |

The limiting masses given above are only indicative, and approximately apply to massive stars of Population I composition ($Z \sim 0.02$). Since mass-loss rates decrease with decreasing $Z$, the mass limits are higher for stars of lower metallicity. The relation of the final evolution stage to the supernova types indicated above will be discussed in Chapter 13.

The scenario for the most massive stars is illustrated in Fig. 12.4 for a $60\,M_\odot$ star. After about 3.5 Myr, while the star is still on the main sequence, mass loss exposes layers that formerly belonged to the (large) convective core. Thus CNO-cycling products (nitrogen) are revealed, and the surface He abundance increases at the expense of H. During the very short phase between central H and He burning ($t = 3.7$ Myr), several $M_\odot$ are rapidly lost in an LBV phase. During the first part of core He burning (3.7 – 3.9 Myr) the star appears as a WNL star, and subsequently as a WNE star (3.9 – 4.1 Myr) after mass loss has removed the last H-rich layers outside the H-burning shell. After 4.1 Myr

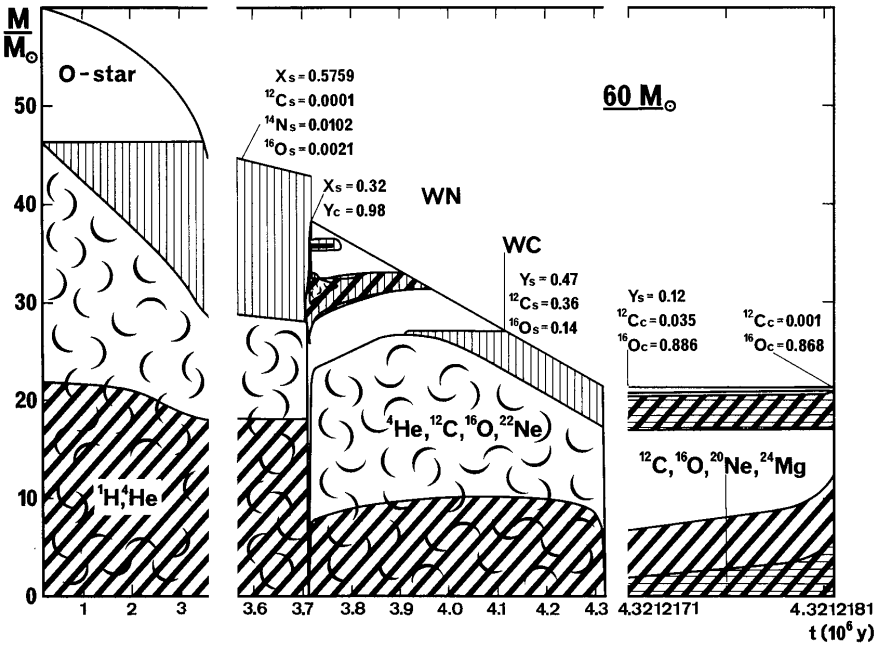


**Figure 12.4.** Kippenhahn diagram of the evolution of a $60\,M_\odot$ star at $Z = 0.02$ with mass loss. Cross-hatched areas indicate where nuclear burning occurs, and curly symbols indicate convective regions. See text for details. Figure from Maeder & Meynet (1987).

material that was formerly in the He-burning convective core is exposed at the surface: N, which was consumed in He-burning reactions, disappears while the products of He-burning, C and O, appear. The last 0.2 Myr of evolution this star spends as a WC star.

In general, mass-loss rates during all evolution phases increase with stellar mass, resulting in timescales for mass loss that are less that the nuclear timescale for $M \gtrsim 30\,M_\odot$. As a result, there is a *convergence* of the final (pre-supernova) masses to $\sim 5 - 10\,M_\odot$. However, this effect is much diminished for metal-poor stars because the mass-loss rates are generally lower at low metallicity.

## 12.3 Advanced evolution of massive stars

The evolution of the surface properties described in the previous section corresponds to the hydrogen and helium burning phases of massive stars. Once a carbon-oxygen core has formed after He burning, which is massive enough ($> 1.06\,M_\odot$) to undergo carbon ignition, the subsequent evolution of the *core* is a series of alternating nuclear burning and core contraction cycles in quick succession (see Fig. 12.5). The overall evolution trend is an increase of central temperature and central density, roughly following $T_c \propto {\rho_c}^{1/3}$ as expected from homologous contraction in our schematic evolution picture (Chapter 8). For central temperatures $\gtrsim 5\times10^8$ K, the evolution tracks deviate from this trend, sloping towards somewhat higher $\rho_c$ and lower $T_c$. This is the result of cooling of the core by strong *neutrino emission* (see Sect 12.3.1).

The main effect of neutrino energy losses, however, is not visible in Fig. 12.5: they speed up the evolution of the core enormously. Less than a few thousand years pass between the onset of carbon burning until the formation of an iron core. During this time the mass of the C-O core remains fixed. Furthermore, the stellar *envelope* hardly has time to respond to the rapid changes in the core, with the consequence that the evolution of the envelope is practically disconnected from that of the core. As a result the position of a massive star in the HR diagram remains almost unchanged during carbon burning and beyond. We can thus concentrate on the evolution of the core of the star from this point onwards.

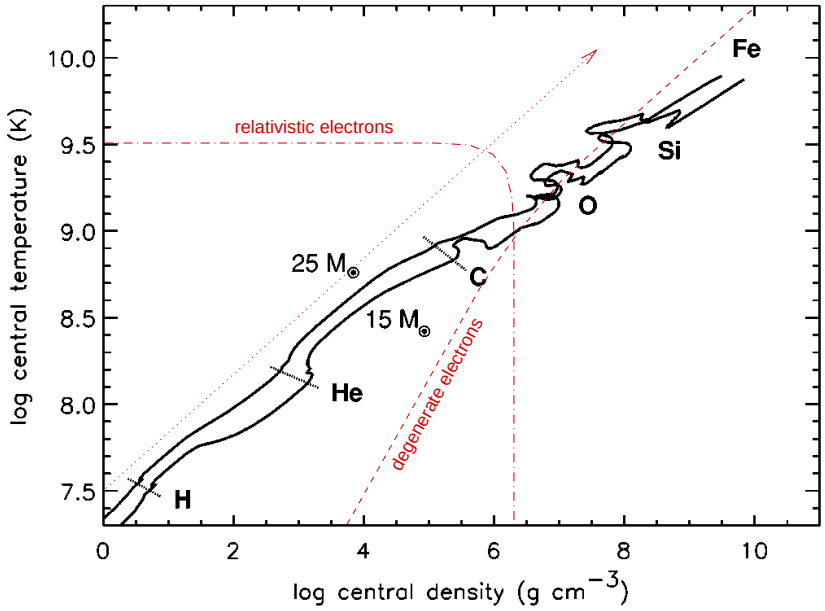


**Figure 12.5.** Evolution of central temperature and density of 15 $M_\odot$ and 25 $M_\odot$ stars at $Z = 0.02$ through all nuclear burning stages up to iron-core collapse. The dashed line indicated where electrons become degenerate, and the dash-dotted line shows where electrons become relativistic ($\epsilon_e \approx m_e c^2$). The dotted line and arrow indicates the trend $T_c \propto {\rho_c}^{1/3}$ that is expected from homologous contraction. Non-monotonic (non-homologous) behaviour is seen whenever nuclear fuels are ignited and a convective core is formed. Figure adapted from Woosley, Heger & Weaver (2002, Rev. Mod. Ph. 74, 1015).

### 12.3.1 Evolution with significant neutrino losses

In Sect. 6.5 we discussed several weak interaction processes that result in spontaneous neutrino emission at high temperatures and densities, such as photo-neutrinos, plasma-neutrinos and pair annihilation neutrinos. When the central temperature exceeds $\sim 5 \times 10^8$ K, these neutrino losses are the most important *energy leak* from the stellar centre, taking away energy much more rapidly than photon diffusion or even convection can transport it to the surface. From this point onwards the neutrino luminosity from the core far exceeds the luminosity radiated from surface, $L_\nu \gg L$.

The dependence of the nuclear energy generation rate $\epsilon_{\rm nuc}$ and the neutrino loss rate $\epsilon_\nu$ on temperature are depicted in Fig. 12.6, for the centre of a typical massive star (i.e. following an evolution track approximating those shown in Fig. 12.5). Both $\epsilon_\nu$ and $\epsilon_{\rm nuc}$ increase strongly with temperature, but the $T$-dependence of $\epsilon_{\rm nuc}$ is larger than that of $\epsilon_\nu$. During nuclear burning cycles energy production and neutrino cooling are in balance, $\epsilon_{\rm nuc} = \epsilon_\nu$, and this condition (the intersection of the two lines) defines the temperature at which burning takes place.[1]

During each nuclear burning phase, $L_{\rm nuc} = \dot{E}_{\rm nuc} \approx L_\nu$, which thus results in a much shorter nuclear timescale than if neutrino losses were absent: $\tau_{\rm nuc} = E_{\rm nuc}/L_\nu \ll E_{\rm nuc}/L$. Similarly, in between burning cycles the rate of core contraction (on the thermal timescale) speeds up: $\dot{E}_{\rm gr} \approx L_\nu$ so that $\tau_{\rm th} = E_{\rm gr}/L_\nu \ll E_{\rm gr}/L$. Therefore the evolution of the core speeds up enormously, at an accelerating rate as the core continues to contract and heat up. The lifetime of each nuclear burning stage can be estimated from Fig. 12.6 by approximating $\tau_{\rm nuc} \sim q/\epsilon_{\rm nuc}$, where $q$ is the energy gain per unit mass from nuclear burning ($\sim 4.0, 1.1, 5.0$ and $1.9 \times 10^{17}$ erg/g for C-, Ne-, O- and Si-burning,

[1] Note that because $\epsilon_{\rm nuc}$ is a steeper function of $T$ than $\epsilon_\nu$, nuclear burning is stable also in the presence of neutrino losses: a small perturbation $\delta T > 0$ would increase the local heat content ($\epsilon_{\rm nuc} > \epsilon_\nu$), leading to expansion and cooling of the core until thermal equilibrium is re-established.

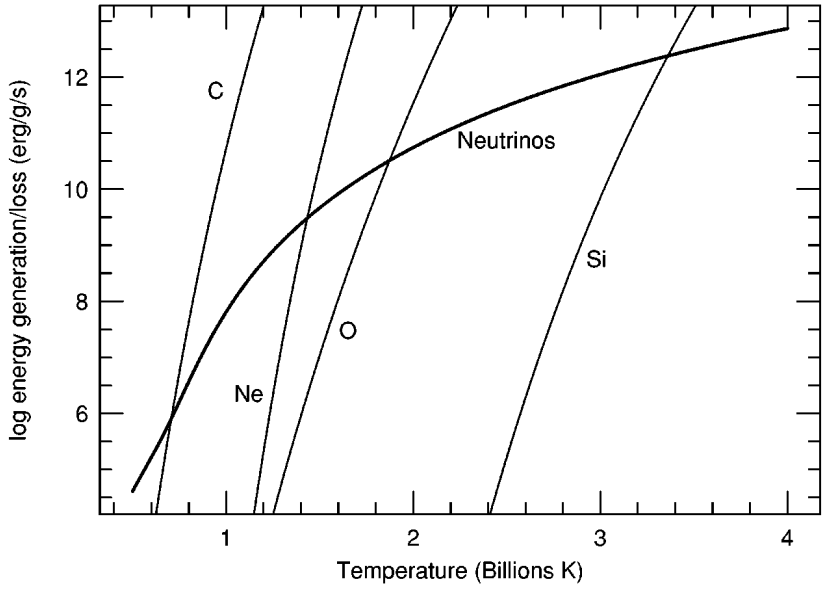


**Figure 12.6.** Energy generation rate and neutrino loss rate during the advanced evolution of a massive star. The stellar center is assumed to follow a track approximating that shown in Fig. 12.5. The intersections of the nuclear burning lines with the neutrino loss line define the burning temperature of the corresponding fuel. Figure from Woosley, Heger & Weaver (2002).

respectively) and $\epsilon_{\rm nuc}$ is the energy generated per gram and per second at the intersection with $\epsilon_\nu$ in Fig. 12.6. Thus the lifetime ranges from several $10^3$ years for C-burning to about a day for Si-burning!

### 12.3.2 Nuclear burning cycles: carbon burning and beyond

When the temperature in the contracting C-O core reaches $5 - 8 \times 10^8$ K (depending on the mass of the core), carbon is the first nuclear fuel to be ignited. The reactions involved in carbon burning and further nuclear burning cycles were treated in Sec. 6.4.3. In the following sections we briefly review these and discuss the consequences for the structure and evolution of the star. A typical example of the interior evolution is shown in Fig. 12.7 for a 15 $M_\odot$ star, and the corresponding stellar properties are given in Table 12.1.

**Table 12.1.** Properties of nuclear burning stages in a 15 $M_\odot$ star (from Woosley et al. 2002).

| burning stage | $T$ ($10^9$ K) | $\rho$ (g/cm$^3$) | fuel | main products | timescale |
|---|---|---|---|---|---|
| hydrogen | 0.035 | 5.8 | H | He | $1.1 \times 10^7$ yr |
| helium | 0.18 | $1.4 \times 10^3$ | He | C, O | $2.0 \times 10^6$ yr |
| carbon | 0.83 | $2.4 \times 10^5$ | C | O, Ne | $2.0 \times 10^3$ yr |
| neon | 1.6 | $7.2 \times 10^6$ | Ne | O, Mg | 0.7 yr |
| oxygen | 1.9 | $6.7 \times 10^6$ | O, Mg | Si, S | 2.6 yr |
| silicon | 3.3 | $4.3 \times 10^7$ | Si, S | Fe, Ni | 18 d |

### Carbon burning

Carbon burning proceeds via the $^{12}C + {}^{12}C$ reaction, which produces a mixture of products, mainly $^{20}Ne$ and some $^{24}Mg$. Most of the energy produced escapes in the form of neutrinos and only a small fraction is carried away by photons. In stars with masses up to about 20 $M_\odot$ the photon luminosity is large enough to produce a convective core (as shown in Fig. 12.7) of about 0.5 $M_\odot$. In more massive stars carbon burns radiatively, because the initial $^{12}C$ abundance is smaller and the luminosity not

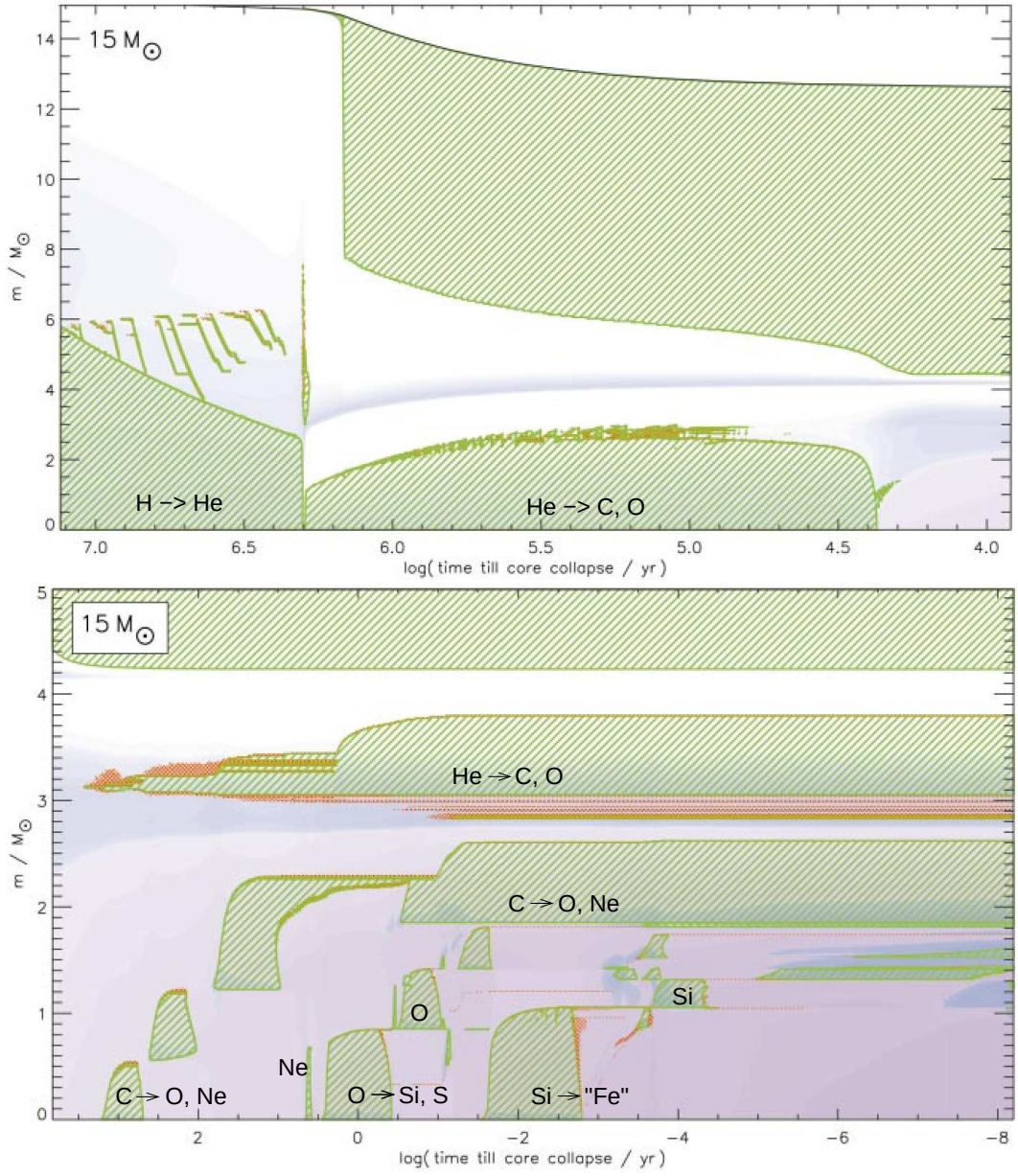


**Figure 12.7.** Kippenhahn diagram of the evolution of a 15 $M_\odot$ star showing convective regions (cross-hatching) and nuclear burning intensity (blue shading) during central H and He burning (top panel) and during the late stages in the inner 5 $M_\odot$ of the star (bottom panel). A complicated series of convective burning cores and shells appear, due to respectively carbon burning (around $\log t \sim 3$), neon burning (around $\log t \sim 0.6$), oxygen burning (around $\log t \sim 0$) and silicon burning (around $\log t \sim -2$). Figure from Woosley, Heger & Weaver (2002.)

carried away by neutrinos can all be transported by radiation. The duration of the C-burning phase is of the order of $10^3$ yrs. It should be noted that these results are sensitive to the uncertain rate of the $^{12}C(\alpha,\gamma)^{16}O$ rate, which determines the $^{12}C$ abundance left after He-burning – a lower rate will leave more $^{12}C$ to be burned and this increases both the size of the convective core and the duration of the C-burning phase.

Following carbon exhaustion in the centre, the core – which is now composed mostly of O and Ne – contracts on its neutrino-accelerated Kelvin-Helmholtz timescale and carbon burning continues in a convective shell around this core. Several such convective shell-burning episodes can occur in succession, as shown in Fig. 12.7, their number depending on the mass of the star. The discrete nature of these shell burning events can also produce a discrete (discontinuous) dependence of the final state of the core on the initial stellar mass.

In stars with masses up to about $11\,M_\odot$ (C-O core masses less than $1.38\,M_\odot$) carbon burning proceeds somewhat differently. The C-O core becomes partially degenerate and neutrino losses effectively cool the centre of the star, so that carbon does not ignite in the centre but in an off-centre shell in a mildly degenerate flash (analogous to, but much less violent than the He flash in low-mass stars). After one or more of these mild carbon flashes the burning front moves to the centre and stable carbon burning in a convective core follows. After carbon burning, the O-Ne core becomes degenerate and no further nuclear fuels are ignited. The structure of these stars is then very similar to those of AGB stars with degenerate CO cores, discussed in Ch. 11, and such stars have been named *super-AGB stars*. The fate of such stars is uncertain and depends on whether the O-Ne core can reach the Chandrasekhar limit by shell burning. If this is the case the core eventually collapses, producing a supernova explosion. On the other hand, if mass loss is strong enough to remove the envelope before the Chandrasekhar limit is reached, the final remnant is a O-Ne white dwarf.

**Neon and oxygen burning**

In stars with masses $\gtrsim 11\,M_\odot$, once the temperature in the contracting O-Ne core reaches $\approx 1.5{\times}10^9$ K neon is 'burned' into oxygen and magnesium by a combination of photo-disintegration and $\alpha$-capture reactions (Sec. 6.4.3). Neon burning always occurs in a convective core, regardless of stellar mass. By this time increased neutrino losses have accelerated the rate of evolution by a factor $\sim 10^3$ compared to the carbon-burning phase (see Fig. 12.6). The duration of the neon-burning phase is therefore very short, of order 1 year. Neon burning then shifts to a shell, as was the case for carbon burning, but in this case the time left until the next fuel is ignited is so short that no significant shell burning occurs.

When $T_9 \approx 2.0$ oxygen is ignited in the core by means of the $^{16}O + {}^{16}O$ reaction, producing mostly $^{28}Si$ and $^{32}S$ with a significant admixture of other isotopes (see below). Oxygen burning also occurs in a convective core, with a typical mass of $\approx 1.0\,M_\odot$ (see Fig. 12.7). The duration is somewhat longer than that of neon burning, of order 1 year, despite the higher neutrino loss rate at this stage. The reasons for this longer duration are the large oxygen mass fraction, $\sim 0.7$, and the large energy gain per gram compared to Ne burning. Similar to carbon burning, after central oxygen burning a number of convective oxygen-burning shells appears in quick succession. By this point the remaining time until core collapse ($< 1$ yr) is so short that the overlying helium- and carbon-burning shells remain frozen into the stellar structure.

Apart from $^{28}Si$ and $^{32}S$, oxygen burning produces several neutron-rich nuclei such as $^{30}Si$, $^{35}S$ and $^{37}Cl$. Partly these result from $\alpha$-captures on n-rich isotopes already present during C-burning, and partly from weak interactions (electron captures) such as $^{30}P(e^-,\nu)^{30}Si$. As a result the overall number of neutrons in the remnant Si-S core exceeds the number of protons (n/p $> 1$) and therefore that of electrons (implying that $\mu_e > 2$).

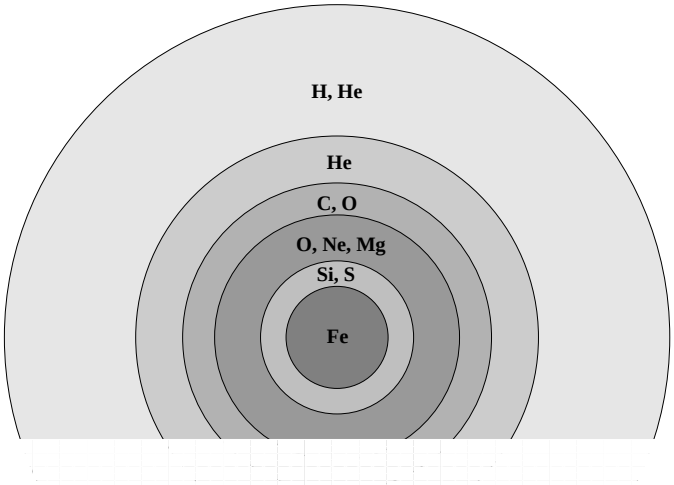


**Figure 12.8.** Schematic overview of the onion-skin structure of a massive star at the end of its evolution.

**Silicon burning**

When the central temperature exceeds $3 \times 10^9$ K, a process known as silicon burning starts. Rather than a fusion reaction this is a complex combination of photo-disintegration and $\alpha$-capture reactions. Most of these reactions are in equilibrium with each other, and their abundances can be described by nuclear equivalents of the Saha equation for ionization equilibrium. For $T > 4 \times 10^9$ K a state close to *nuclear statistical equilibrium* (NSE) can be reached, where the most abundant nuclei are those with the lowest binding energy, i.e. isotopes belonging to the *iron group*. The abundances are further constrained by the total number of neutrons and protons present. Due to the neutron excess of the oxygen burning ashes (see above), the final composition is mostly $^{56}$Fe and $^{52}$Cr.

Silicon burning also occurs in a convective core of $\approx 1\,M_\odot$ and its duration is extremely short, of order $10^{-2}$ yr. As in previous phases, several convective shell-burning episodes usually follow in quick succession. The precise extent and number of these convective events determines the exact value of the final mass of the *iron core*, which has important consequences for the following core collapse and supernova phase (see Sec. 13.2).

### 12.3.3 Pre-supernova structure

We have obtained the following general picture of the final stages in the life of a massive star. The C-O core left by helium burning goes through a rapid succession of nuclear burning stages, during which the stellar envelope (and the star's position in the H-R diagram) remains largely unchanged. After the exhaustion of a fuel (e.g. carbon) in the centre, the remaining core contracts and burning continues in a surrounding shell. Neutrino losses speed up the contraction and heating of the core, until the next fuel (e.g. neon) is ignited in the centre. At each subsequent burning stage the outer burning shells have advanced outward, while neutrino cooling has become more efficient, resulting in a smaller burning core (in mass) than during the previous stage. Eventually this leads to an *onion-skin* structure, depicted schematically in Fig. 12.8. The star is composed of different concentric shells, which consist of heavier nuclei as one moves from the from the envelope towards the centre, and which are separated by burning shells. Often the nuclear burning, both in the centre and in shells, causes convective regions to appear that partially mix the various onion-skin layers. This leads to rather complicated abundance profiles at the moment when the inner core has gone through silicon burning and is composed of iron-group elements. An example of this structure is shown in Fig. 12.9 for a $15\,M_\odot$ star.

At this point the mixture of nuclei in the inner core has reached the minimum possible nuclear binding energy, given the ratio of neutrons to protons that is present, i.e. the composition is mainly

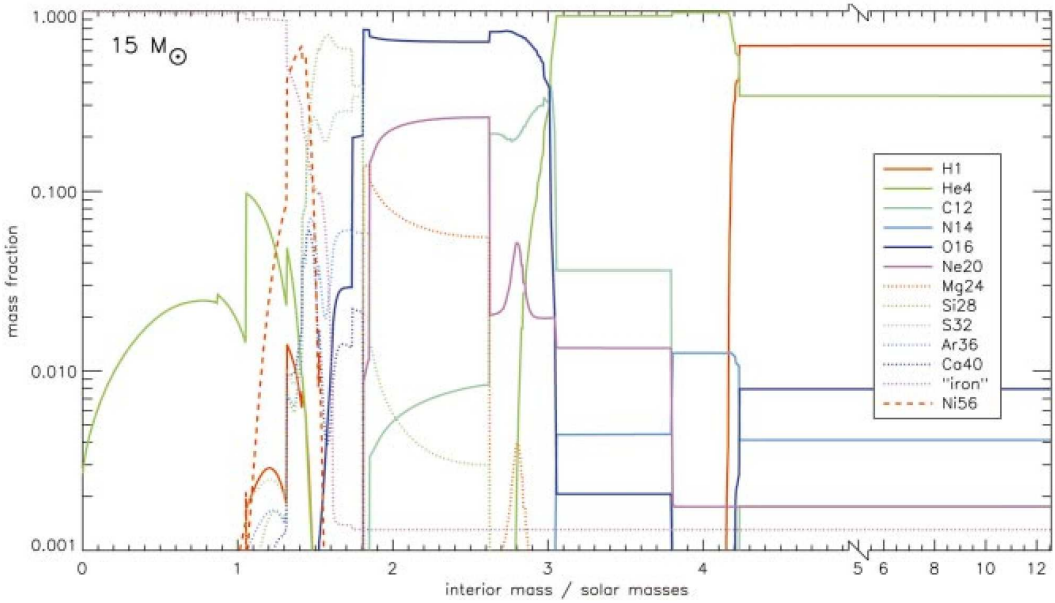


**Figure 12.9.** Final composition profiles of a 15 $M_\odot$ star (see Fig. 12.7), just before core collapse. "Iron" refers to the sum of neutron-rich nuclei of the iron group, especially $^{56}$Fe. Figure from Woosley, Heger & Weaver (2002).

$^{56}$Fe. From this iron core no further energy can be extracted by nuclear fusion: it has become inert. The iron core rapidly becomes unstable and starts collapsing, giving rise to a supernova explosion. The collapse of the core and its consequences are discussed in the next chapter.

---

## Suggestions for further reading

The evolution of massive stars, including the effects of mass loss and rotation, is treated in detail in Chapters 27 and 28.1-4 of Maeder. A thorough review of the current state of our understanding of the evolution of massive stars, their explosions and nucleosynthesis is given by Woosley, Heger & Weaver (2002, Rev. Mod. Ph., 74, 1015). Several of the figures from this article are reproduced in this chapter.

---

## Exercises

**12.1 Mass loss of massive stars during the main sequence**

The mass-luminosity relation for massive stars on the main sequence is approximately

$$\log\left(\frac{L}{L_\odot}\right) \approx 0.781 + 2.760 \times \log\left(\frac{M_i}{M_\odot}\right),$$

where $M_i$ is the initial mass. The mass loss rate of massive stars can roughly be approximated by

$$\log \dot{M} \approx -12.76 + 1.3 \times \log\left(\frac{L}{L_\odot}\right).$$

The duration of the main sequence phase $\tau_{\rm MS}$ in years is approximately

$$\log \tau_{\rm MS} \approx 7.719 - 0.655 \times \log\left(\frac{M_i}{M_\odot}\right).$$

(a) Calculate the fraction of mass that is lost by massive stars with $M_i = 25, 40, 60, 85$ and $120\,M_\odot$ during the main sequence phase.

(b) A star with an initial mass of $85\,M_\odot$ on the zero age main sequence has a convective core that contains 83 % of the mass. Calculate the time at which products of nuclear burning will appear at the surface.

(c) *Wolf-Rayet* (WR) stars are massive stars that have lost practically their complete hydrogen rich envelope. They can be classified according to their surface abundances:

**WC** No hydrogen, high abundances of He, C and O

**WNE** No Hydrogen, N/He ratio consistent with CNO equilibrium

**WNL** Some Hydrogen, N/He ratio consistent with CNO equilibrium

Put the sub-classifications in 'chronological order'. What type of WR is the star in question b)?

### 12.2 Maximum mass loss rate for a radiation driven wind

(a) Assume that all photons transfer their entire *momentum* to the outflowing wind. Show that the maximum mass loss rate that can be driven by radiation is given by

$$\dot{M} < \dot{M}_{\rm max} = \frac{L}{v_\infty c},$$

where $v_\infty$ is the velocity of the wind at a large distance of the star.

(b) Show that with this maximum mass loss rate, the *kinetic energy* of the wind is only a small fraction of the luminosity, i.e.

$$\frac{1}{2}\dot{M}_{\rm max} v_\infty^2 \ll L \quad (v_\infty \approx 3 v_{\rm esc})$$

### 12.3 Burning stages

(a) Explain why the timescales of the burning stages from C-burning onward are very short compared to the H- and He-burning phases.

(b) Why does neon burning precede oxygen burning (why does it occur at a lower temperature) even though $^{20}$Ne is a heavier nucleus than $^{16}$O?

(c) The end result of nuclear burning in a massive star is an onion-like structure of the ashes of the various nuclear burning stages. Try to identify these layers, and the nuclear reactions that are responsible for them, in Figure 12.9.

# Chapter 13

# Stellar explosions and remnants of massive stars

## 13.1 Supernovae

Supernovae are stellar explosions during which the luminosity of a star reaches $10^9 - 10^{10}\,L_\odot$ at maximum, remaining bright for several months afterward. At least eight supernovae have been observed in our Galaxy over the past 2000 years, by Chinese and in some cases also by Japanese, Korean, Arabian and European astronomers (see Table 13.1). The remnants of these supernovae are in most cases still visible as luminous expanding nebulae, containing the matter that was expelled in the explosion. The supernova that left the remnant known as Cas A has not been reported, its explosion date has been inferred from the expansion rate of the nebula. Recently, however, the *light echo* of this supernova, as well as that of Tycho's supernova of 1572, have been detected from which the supernova type has been determined. No supernova is known to have occurred in our Galaxy in the last 340 years. Most of our observational knowledge comes from extragalactic supernovae, the first of which was discovered in 1885 in the Andromeda galaxy, and which are currently discovered at a rate of several hundred per year thanks to dedicated surveys. A Galactic supernova rate of about 1 every 30 years has been inferred from this.

**Table 13.1.** Historical supernovae.

| year (AD) | $V$ (peak) | SN remnant | SN type | compact object |
|---|---|---|---|---|
| 185 | −2 | RCW 86 | Ia? | – |
| 386 | | ? | ? | |
| 393 | −3 | ? | ? | |
| 1006 | −9 | PKS 1459-41 | Ia? | – |
| 1054 | −6 | Crab nebula | II | NS (pulsar) |
| 1181 | −1 | 3C 58 | II | NS (pulsar) |
| 1572 | −4 | 'Tycho' | Ia | – |
| 1604 | −3 | 'Kepler' | Ia? | – |
| ~1667 | $\gtrsim$+6 | Cas A | IIb | NS |

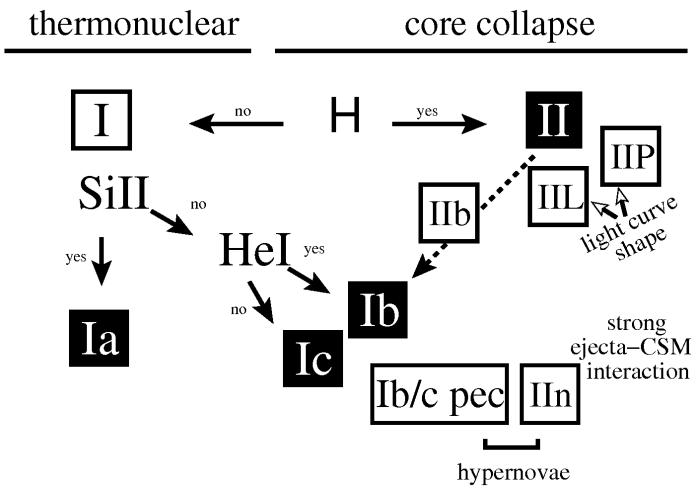


**Figure 13.1.** Classification of supernovae, based on their spectra and lightcurve shapes. The main supernova types are shown as black squares. Figure from Turatto (2003, LNP 598, 21).

**Supernova classification**

On the basis of their spectra, supernovae (SNe) have been historically classified into Type I (those that do not show hydrogen lines) and Type II (those that do). A more detailed classification scheme that is currently used, is shown in Fig. 13.1.

**Type Ia** The main spectral features are the lack of H lines and the presence of strong Si II lines around maximum brightness. After several months, lines of Fe and Co appear in the spectra. Type Ia supernovae occur in galaxies of all types, including elliptical galaxies which only contain old stellar populations, indicating that SNe Ia can have long-lived, low-mass progenitors. They are caused by the *thermonuclear explosion* of a CO white dwarf that reaches the Chandrasekhar limit $M_{\rm Ch}$ by mass accretion in a binary system (see Sec. 13.3). About 25–30% of observed supernovae are of Type Ia. They are (on average) the most luminous of all supernova types and their lightcurves (see Fig. 13.2) form a rather homogeneous group, which makes them of great interest as cosmological probes.

**Type II** The spectra of Type II supernovae are dominated by H lines, while lines of Ca, O and Mg are also present. SNe II occur in the spiral arms of galaxies where star formation takes place, and therefore correspond to the explosion of massive stars with short lifetimes. With about 50% of all supernovae, these are the most common type of stellar explosion. SNe II form the main class of explosions associated with the *core collapse* of massive stars that have hydrogen-rich envelopes. In several cases, the progenitor stars of Type II supernovae have been detected before the explosion. With the notable exception of SN 1987A (see Sec. 13.2.3), these progenitor stars were *red supergiants* with masses $8\,M_\odot \lesssim M \lesssim 16\,M_\odot$.

Type II supernovae show a variety of lightcurve shapes (Fig. 13.2), on the basis of which they are often sub-classified into **Type II-P** (showing, after an initial rapid rise and decline in brightness, a long 'plateau' phase of almost constant luminosity lasting 2–3 months, before a slow exponential decay) and **Type II-L** (which lack the plateau phase). In addition, one distinguishes **Type IIb**, in which the spectral signatures change from Type II to Type Ib (see below); and **Type IIn**, showing narrow emission lines on top of broad emission lines, which are interpreted as resulting from heavy mass loss prior to the explosion.

**Type Ib and Ic** Type Ib supernovae have strong He lines in their spectra, which are lacking in Type Ic supernovae. Both types show a lack of hydrogen, and strong lines of O, Ca and Mg are present.

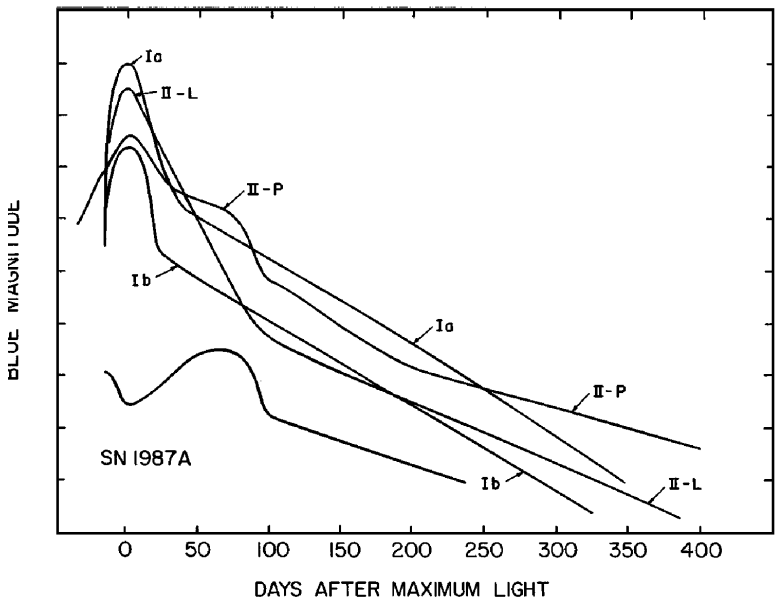


**Figure 13.2.** Schematic supernova lightcurves. Typical maximum *B*-band magnitudes are −19.5 for SNe Ia, −17.6 for both SNe Ibc and II-L, and −17.0 for SNe II-P. The lightcurves of SNe Ic resemble those of SNe Ib. Figure from Filippenko (1997, ARA&A 35, 309).

Similar to SNe II, they are found in star-forming regions, and their late-time spectra are also similar to Type II. Hence Type Ib/c supernovae are also associated with core collapse of massive stars, namely those that have lost their H-envelopes prior to explosion. Together they constitute about 20% of all supernovae. A subclass of very bright Type Ic supernovae, known as *hypernovae*, may be associated with gamma-ray bursts.

## 13.2 Core collapse and explosion of massive stars

As indicated in Fig. 13.1, essentially all types of supernova – except Type Ia – appear to be associated with the core collapse of massive stars ($\gtrsim 8\,M_\odot$) at the end of their evolution. The distinction between the different types and subtypes of core-collapse supernovae is related to differences in the structure and composition of the envelopes of the progenitor stars. For example, the progenitors of Type II supernovae are still surrounded by a massive H-rich envelope at the moment of explosion, while SN Ib progenitors have lost their H-rich envelopes and SN Ic progenitors have also lost most of the He layers surrounding the core. This sequence can be the consequence of mass loss from stars of increasing initial mass (see Sec. 12.2), but can also result from interaction with a binary companion.

### 13.2.1 The collapse of the iron core

Despite these differences in appearance, the *physical mechanism* is similar in all core-collapse supernovae. We have seen in Sec. 12.3.3 that stars with $M \gtrsim 11\,M_\odot$ form an inner core composed of iron-group elements (mostly $^{56}$Fe) at the end of their evolution. From this iron core no further energy can be extracted by nuclear fusion: it has become inert.

The iron core is in a peculiar state in several respects. Because of neutrino cooling during the late evolution stages, the core typically has a considerable degree of electron degeneracy, except for the largest stellar masses (see Fig. 12.5). However, the high temperature and density ($\gtrsim 10^9$ g/cm$^3$) mean that the electrons are always relativistic (their typical energy exceeds $m_e c^2$). In that case contraction cannot be stopped, even if the core is degenerate, and must continue on the very rapid, neutrino-mediated thermal timescale. Furthermore, since the relativistic electron gas dominates the pressure,

the adiabatic exponent $\gamma_{\rm ad}$ is close to $\frac{4}{3}$. The iron core is therefore very close to a state of dynamical instability. Two processes occur at high density and temperature that contribute to accelerating the (already rapid) contraction into a dynamical collapse of the core.

**Electron captures** At very high density free electrons can be captured and bound into otherwise $\beta$-unstable heavy nuclei. This process, also known as inverse $\beta$-decay, occurs when the most energetic electrons have energies high enough to overcome the difference in nuclear binding energy (see also Sec. 11.2). As a result, the composition becomes increasingly neutron-rich – a process known as *neutronization*. Furthermore, the electron pressure decreases which can destroy the precarious state of hydrostatic equilibrium and trigger the collapse of the core.

If the core is significantly degenerate, the Chandrasekhar mass plays an important role. For a composition of predominantly $^{56}$Fe one would expect $M_{\rm Ch} = 5.83\,\mu_{\rm e}^{-2}\,M_\odot \approx 1.26\,M_\odot$. Electron captures increase the average mass per free electron ($\mu_{\rm e}$) and thus decrease the effective Chandrasekhar mass. This can bring the core mass above this critical mass and facilitate its collapse.

Electron captures can also trigger the collapse of stars with initial masses below $\approx 11\,M_\odot$, which develop degenerate O-Ne cores at the end of their lives. If the mass of this core can grow (through shell burning) to $1.37\,M_\odot$, electrons are captured by $^{24}$Mg and $^{20}$Ne which initiates the collapse of the core. Stellar explosions caused by this mechanism are called *electron-capture supernovae*.

**Photo-disintegration** If the temperature in the contracting core reaches values close to $10^{10}$ K, the energy of the photons becomes large enough to break up the heavy nuclei into lighter ones, in particular $^{56}$Fe is disintegrated into $\alpha$ particles and neutrons:

$$^{56}\mathrm{Fe} + \gamma \leftrightarrow 13\,{}^4\mathrm{He} + 4\,\mathrm{n} \tag{13.1}$$

This reaction is in statistical equilibrium and the abundances of the nuclei involved are determined by a Saha-type equation, the balance shifting more towards the right-hand side the higher the temperature. The process is thus similar to the ionization of hydrogen, and results in lowering $\gamma_{\rm ad}$ to below the critical value of $\frac{4}{3}$. The core therefore becomes dynamically unstable. This process dominates in relatively massive iron cores.

The photo-disintegration of $^{56}$Fe requires a lot of energy, about 2 MeV per nucleon. This energy is absorbed from the radiation field and thus ultimately from the internal energy of the gas. As a result the pressure decreases quite drastically, triggering an almost free-fall collapse of the core.

The collapse is extremely rapid, taking of the order of 10 msec, because of the short dynamical timescale at the high density ($\sim 10^{10}$ g/cm$^3$) when the collapse is initiated. During the collapse the temperature and pressure keep rising, but never enough to reverse the collapse until nuclear densities are reached. Further photo-disintegrations can occur due to the increasing photon energies, which was once thought (prior to 1980) to dissociate even the $\alpha$ particles completely into free protons and neutrons ($^4\mathrm{He} + \gamma \rightarrow 2\,\mathrm{p} + 2\,\mathrm{n}$, which would require another 7 MeV per nucleon of internal energy from the gas). It has since become clear that full dissociation of $^{56}$Fe into $\alpha$ particles and free nucleons does not occur during the collapse. On the other hand, electron captures onto protons ($\mathrm{p} + \mathrm{e}^- \rightarrow \mathrm{n} + \nu$) inside the heavy nuclei continue the process of neutronization, creating more and more neutron-rich nuclei. These eventually merge, creating what is essentially a gigantic stellar-mass nucleus, when $\rho$

approaches nuclear densities of the order $10^{14}\,\mathrm{g/cm^3}$. The composition inside the core is predominantly neutrons, which become degenerate and thereby modify the equation of state to suddenly become 'stiff', i.e. the neutron gas becomes almost incompressible. This terminates the collapse at a core radius of $R_\mathrm{c} \approx 20\,\mathrm{km}$.

**Energetics of core collapse and supernova explosion**

The gravitational energy released during the collapse of the core can be estimated as

$$E_\mathrm{gr} \approx -\frac{GM_\mathrm{c}^2}{R_\mathrm{c,i}} + \frac{GM_\mathrm{c}^2}{R_\mathrm{c,f}} \approx \frac{GM_\mathrm{c}^2}{R_\mathrm{c,f}} \approx 3 \times 10^{53}\,\mathrm{erg}, \tag{13.2}$$

assuming homologous collapse of a core of $M_\mathrm{c} \approx 1.4\,M_\odot$ from an initial radius $R_\mathrm{c,i} \sim 3000\,\mathrm{km}$ to a final radius $R_\mathrm{c,f} \approx 20\,\mathrm{km} \ll R_\mathrm{c,i}$. Let us compare this with the energy necessary to expel the envelope, which has no time to follow the core collapse,

$$E_\mathrm{env} = \int_{M_\mathrm{c}}^{M} \frac{Gm}{r}\,dm \ll \frac{GM^2}{R_\mathrm{c,i}}. \tag{13.3}$$

The upper limit (13.3) is $\approx 10^{53}\,\mathrm{erg}$ for $M = 10\,M_\odot$, but taking into account a realistic mass distribution in the envelope, this estimate comes down to $E_\mathrm{env} \sim 10^{50}\,\mathrm{erg}$. Only a very small fraction of the energy released in the collapse of the core is needed to blow away the envelope. Part of the energy goes into kinetic energy of the ejected envelope and energy radiated away by the supernova. For a typical Type II supernova, the ejected envelope is $\sim 10\,M_\odot$ and observed ejecta velocities are about $10^4\,\mathrm{km/s}$, giving $E_\mathrm{kin} \sim 10^{51}\,\mathrm{erg}$. The supernova has a luminosity $L \approx 2 \times 10^8\,L_\odot$ for up to several months, so that the total energy lost in the form of radiation is $E_\mathrm{ph} \sim 10^{49}\,\mathrm{erg}$. Therefore

$$E_\mathrm{ph} \sim 0.01 E_\mathrm{kin} \sim 10^{-4} E_\mathrm{gr} \qquad \text{and} \qquad E_\mathrm{gr} \gg E_\mathrm{env} + E_\mathrm{kin} + E_\mathrm{ph},$$

such that only a small fraction of the energy released in the collapse is used in the actual explosion. The question is how this fraction of about 1% of the gravitational energy can be converted into kinetic energy of the envelope, which turns out to be a very difficult problem.

### 13.2.2 The explosion mechanism

When the collapsing core reaches nuclear densities ($\rho_\mathrm{nuc} \approx 3 \times 10^{14}\mathrm{g/cm^3}$) the neutrons become degenerate, resulting in a strong increase in pressure. Furthermore, nuclear forces between the nucleons become important. These effects reverse the collapse. When the inner part of the core is compressed to $\sim 1.5$ times nuclear density, it bounces back like a spring – an event named *core bounce*.

As the velocity of the inner core material is reversed, it encounters matter from the still free-falling outer part of the core. If the collision were perfectly elastic, the outer core would bounce back to its initial radius even if the inner core were stationary. The outward motion of the inner core thus gives the possibility of a 'super-elastic' core bounce that might conceivably explode the star. The impact of the infalling matter is supersonic and creates a shock wave that steepens as it travels outward into regions of lower density. The kinetic energy stored in the shock wave was once thought to be sufficient to blow off the envelope, giving rise to a so-called *prompt explosion*. However, two problems arise that prevent such a prompt explosion to occur.

First, as the shock wave travels through the infalling matter which still mostly consists of iron-group nuclei, it heats up the nuclei and disintegrates them effectively into protons and neutrons. We can estimate the energy spent in photo-disintegration by noting that the binding energy of an $^{56}$Fe nucleus is about 9 MeV/nucleon, so that the disintegration of an iron core of $1.4\,M_\odot$ ($1.7 \times 10^{57}$

nucleons) requires about $2 \times 10^{52}$ erg. Note that this amounts to absorbing, during a fraction of a second, practically all of the nuclear energy that was released during the lifetime of the star!

Second, electron captures on the free protons created behind the shock produce energetic neutrinos by means of

$$\mathrm{p} + \mathrm{e}^- \rightarrow \mathrm{n} + \nu.$$

These neutrinos take away the largest fraction, about 90%, of the energy released in the collapse, especially as the shock moves into relatively low-density regions ($< 10^{12}$ g/cm$^3$) from where they can easily escape. In the case of supernova 1987A these neutrinos have been detected (see Sec. 13.2.3). As a result, the shock wave fizzles out before it reaches the envelope of the star and no prompt explosion occurs.

**Effects of neutrinos**

The role played by neutrinos during core collapse requires closer examination. The neutrinos produced *before* the collapse set in had typical energies of the order of the thermal energy of the electrons (see Sect. 12.3.1). During the collapse neutrino production by neutronization (electron captures) dominates. The typical energy of these neutrinos is of the order of the Fermi energy of the relativistic electrons,

$$\frac{E_\nu}{m_\mathrm{e}c^2} \approx \frac{E_\mathrm{F}}{m_\mathrm{e}c^2} = \frac{p_\mathrm{F}}{m_\mathrm{e}c} = \frac{h}{m_\mathrm{e}c}\left(\frac{3}{8\pi}\,\frac{\rho}{\mu_\mathrm{e}m_\mathrm{u}}\right)^{1/3} \approx 10^{-2}\left(\frac{\rho}{\mu_\mathrm{e}}\right)^{1/3}, \tag{13.4}$$

using eq. (3.33) and the relation $\rho = \mu_\mathrm{e} m_\mathrm{u} n_\mathrm{e}$, and with $\rho$ in g/cm$^3$ in the last equality. In the presence of heavy nuclei, the neutrinos interact mainly through so-called coherent scattering with these nuclei, with a typical cross section of the order

$$\sigma_\nu \approx 10^{-45} A^2 \left(\frac{E_\nu}{m_\mathrm{e}c^2}\right)^2 \mathrm{cm}^2, \tag{13.5}$$

which gives together with eq. (13.4),

$$\sigma_\nu \approx 10^{-49} A^2 \left(\frac{\rho}{\mu_\mathrm{e}}\right)^{2/3} \mathrm{cm}^2. \tag{13.6}$$

If $n = \rho/(Am_\mathrm{u})$ is the number density of nuclei, the mean free path $\ell_\nu$ of the neutrinos in the collapsing core can then be estimated as

$$\ell_\nu \approx \frac{1}{n\sigma_\nu} \approx 2 \times 10^{25}\,\frac{1}{\mu_\mathrm{e}A}\left(\frac{\rho}{\mu_\mathrm{e}}\right)^{-5/3} \mathrm{cm}. \tag{13.7}$$

Taking $\mu_\mathrm{e} \approx 2$ and $A \approx 100$, we find with eq. (13.7) that when $\rho/\mu_\mathrm{e} \approx 4 \times 10^9$ g/cm$^3$, the neutrino mean free path $\ell_\nu \approx 10^7$ cm, which is the typical dimension of the collapsing core. Apparently, neutrinos can no longer escape freely at the high densities prevailing in the collapsing core. The core becomes opaque for neutrinos, which can only diffuse out of the core via many scattering events. Towards the end of the collapse phase, when $\rho > 3 \times 10^{11}$ g/cm$^3$, the diffusion velocity even becomes smaller than the infall velocity of the gas, so that neutrinos are *trapped* in the core. Analogous to the photosphere of a star, one can define a 'neutrinosphere' in the outer layers of the core where the density is low enough for the neutrinos to escape. Interior to this, there is a 'neutrino trapping surface' below which the neutrinos are trapped.

The real situation is much more complicated because $\sigma_\nu$ depends on the neutrino energy, so that the neutrino transport problem has to be solved in an energy-dependent way. The congestion of neutrinos in the core causes them to become degenerate (since neutrinos are fermions) with a high Fermi energy. Electron capture becomes less probable, because the new neutrinos have to be raised to the top of the Fermi sea. Neutronization therefore effectively stops when $\rho \approx 3 \times 10^{12}$ g/cm$^3$. Only after some neutrinos have diffused out of the core can further neutronization take place. The process of neutronization therefore takes about 3–10 seconds, while the collapse only takes a few milliseconds.

The deposition of neutrino energy in the core provides an energy source that may revive the shock wave and cause an explosion. Neutrinos diffusing out of the collapsed core (the proto-neutron star) heat the region through which the former shock wave has passed, which stretches from ∼30 km to 100–300 km, and cause it to become convectively unstable. Convection thus provides a way to convert some of the thermal energy from neutrino deposition into kinetic energy. Multi-dimensional hydrodynamical calculations show that the outward force thus created can overcome the ram pressure of the outer layers that are still falling onto the core and launch a successful explosion, but only for rather low initial stellar masses (up to $\sim 11\,M_\odot$).

A recently proposed alternative is that the proto-neutron star becomes unstable to g-mode oscillations, which generate acoustic energy that builds up in the shocked region. These acoustic waves eventually cause an anisotropic explosion, whereby the core still accretes on one side while the explosion occurs in the other direction. The asymmetric explosion that results may help explain the large space velocities of radio pulsars, which indicate that neutron stars receive a 'kick' at birth.

### 13.2.3 Lightcurves of core-collapse supernovae

The main physical parameters that determine the appearance of a supernova are:

- the total kinetic energy imparted by the explosion into the envelope,
- the structure (density profile and chemical composition) of the pre-supernova star, as well as the possible presence of circumstellar material lost by the star earlier in its evolution,
- energy input by decay of radioactive isotopes ejected in the explosion.

As we have estimated above, the typical kinetic energy of the explosion is of the order of $E_{\rm kin} \approx 10^{51}$ erg.[1] Given the uncertainty in the precise physical mechanism that converts ∼1% of the core-collapse energy into an explosion (Sec. 13.2.2), one usually models these explosions by injecting a specified amount of energy at the bottom of the envelope by means of a 'piston'. Both $E_{\rm kin}$ and the mass boundary between core and envelope (or 'mass cut') are uncertain and are usually treated as free parameters.

The visible supernova explosion starts when the shock wave induced by the piston reaches the stellar surface, giving rise to a short pulse (∼30 minutes) of soft X-ray emission. The luminosity then declines rapidly as the stellar surface expands and cools. The expanding envelope remains optically thick for a sufficient amount of time that most of the explosion energy is converted into kinetic energy of the outflow. When the envelope has expanded enough to become optically thin, only ∼1% of the initial kinetic energy has been converted into radiation, as the total amount of energy radiated away in the supernova is about $10^{49}$ erg.

When a massive H-rich envelope is present, the recombination of ionized hydrogen provides an additional source of energy once the envelope has become optically thin and cools efficiently. As the

[1] The quantity of $10^{51}$ erg is sometimes referred to as 'f.o.e.' in the supernova literature, and has recently been defined as a new unit 'bethe' (1 B = $10^{51}$ erg) after Hans Bethe, a pioneer in supernova studies.

envelope keeps expanding, a recombination wave moves inward in mass coordinate, while staying at roughly the same radius and temperature. This gives rise to the plateau phase in the lightcurve of a Type II-P supernova. This phase ends when the recombination wave dies out as it meets the denser material of the inner envelope which expands at smaller velocity ($< 10^3$ km/s). If the H-rich envelope is not massive enough to sustain such a recombination wave, the plateau phase is absent (Type II-L lightcurves).

In the last phase of the supernova the lightcurve is determined by the radioactive decay of isotopes released in the explosion. The main source of radioactive energy is $^{56}$Ni, which undergoes two electron captures to produce stable $^{56}$Fe:

$$^{56}\mathrm{Ni} + \mathrm{e}^- \rightarrow {}^{56}\mathrm{Co} + \nu + \gamma \qquad (\tau_{1/2} = 6.1\,\mathrm{d})$$
$$^{56}\mathrm{Co} + \mathrm{e}^- \rightarrow {}^{56}\mathrm{Fe} + \nu + \gamma \qquad (\tau_{1/2} = 77\,\mathrm{d})$$

The exponential decline of the luminosity after 50–100 days corresponds to the decay of $^{56}$Co. The amount of $^{56}$Ni ejected in the explosion, required to explain the observed lightcurves, is about 0.07 $M_\odot$ for a typical Type II supernova. This puts constraints on the position of the 'mass cut' between the collapsing core and the ejected envelope (the remainder of the $^{56}$Ni synthesized is locked up in the collapsed compact object). The lightcurves of Type Ib and Ic supernovae are completely dominated by this radioactive decay, after the initial luminosity peak caused by shock breakout. Other radioactive isotopes (with longer half-lives than $^{56}$Co) can also play a role in the lightcurve at later stages.

**SN 1987A**

This supernova (Type II) in the Large Magellanic Cloud was the nearest supernova observed since Kepler's supernova in 1604. Its progenitor is known from images taken before the supernova: surprisingly it was a *blue* supergiant, with $L \approx 1.1 \times 10^5\,L_\odot$ and $T_{\rm eff} \approx 16\,000$ K, and a probable initial mass of about 18 $M_\odot$. Its relative faintness at peak magnitude is probably related to the compactness of the progenitor star compared to the red supergiant progenitors of SNe II. SN 1987A is the only supernova from which *neutrinos* have been detected, shortly before the visible explosion. During 10 seconds, detectors in Japan and the USA detected 20 neutrinos with energies between 8 and 40 MeV. These energies and the 10 sec time span correspond to the transformation of an Fe core into a hot proto-neutron star during core collapse (see Sec. 13.2.2).

### 13.2.4 Final masses and remnants

Figure 13.3 shows the possible relation between the initial mass of a star of solar metallicity, the mass just before the moment of explosion and the final mass of the remnant. This figure is based on a particular set of stellar models, and the precise masses are dependent on the assumed mass-loss rates, convective overshooting etc., and also depend on metallicity. The pre-supernova mass is determined by mass loss during the evolution of the star, which becomes important for initial masses $\gtrsim 15\,M_\odot$ (Sec. 12.2). For masses above $\sim$30 $M_\odot$, mass loss is strong enough to remove the H-rich envelope as well part of the material that was inside the He core and even the C-O core, shown as green shading.

The type of stellar remnant left behind depends, first of all, on whether the collapse of the iron core successfully generates a supernova explosion. As discussed above, this is still an area of large uncertainty. Detailed numerical simulations do indicate, however, that a successful explosion is more likely the lower the initial mass of the star, or rather, the lower the mass of its C-O core. Stars with initial masses up to 20 $M_\odot$ probably leave *neutron star* remnants. With increasing mass, the amount of kinetic energy generated by the collapse decreases, while the binding energy of the envelope increases. If only a weak explosion is generated, some of the material ejected may fall back onto the

proto-neutron star. If accretion causes the mass to exceed the maximum possible mass of a neutron star – which is uncertain but probably lies in the range 2–3 $M_\odot$– then the proto-neutron star will collapse and form a *black hole*. The mass limit separating stars that form neutron stars and those that leave black holes is probably in the range 20–25 $M_\odot$, but is sensitive to the details of the explosion mechanism as well as to the maximum neutron-star mass. It is even possible that, due to the non-linear behaviour of mass loss, the relation between initial mass and final remnant is non-monotonic and that stars above a certain mass again leave neutron stars (as suggested in Fig. 13.3). On the other hand, if mass loss is weak and a massive C-O core is left prior to core collapse, a successful supernova shock may not develop at all and the entire star may collapse directly into a black hole.

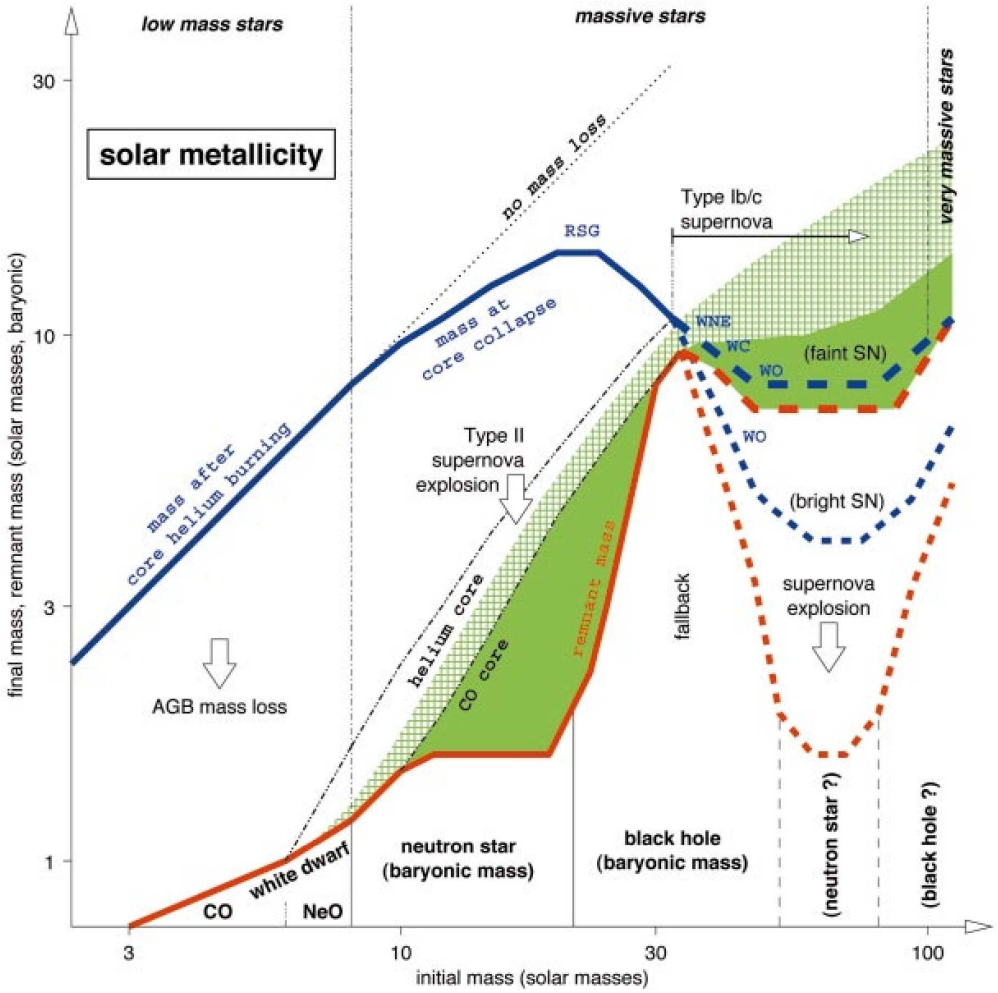


**Figure 13.3.** Initial-final mass relation for stars of solar composition. The blue line shows the stellar mass after core helium burning, reduced by mass loss during earlier phases. For $M \gtrsim 30\,M_\odot$ the helium core is exposed as a WR star, the dashed line gives two possibilities depending on the uncertain WR mass-loss rates. The red line indicates the mass of the compact stellar remnant, resulting from AGB mass loss in the case of intermediate-mass stars, and ejection of the envelope in a core-collapse supernova for massive stars. The green areas indicate the amount of mass ejected that has been processed by helium burning and more advanced nuclear burning. (Figure from Woosley et al. 2002).

## 13.3 Type Ia supernovae

Type Ia supernovae are fundamentally different from other SN types, because they are not associated with the core collapse of massive stars. Instead they are caused by the *thermonuclear explosion* of a CO white dwarf that reaches a critical mass for carbon ignition.

Carbon-burning reactions can occur in a low-temperature degenerate gas if the density is sufficiently high, about $2 \times 10^9$ g/cm$^3$ (these are known as *pycno-nuclear reactions*, see Sec. 6.2.3). These densities are reached in the centre when the mass is very close to the Chandrasekhar mass of 1.4 $M_\odot$. Because the gas is strongly degenerate, carbon burning is unstable and leads to a strong increase in temperature at constant density and pressure. This is analogous to what happens during the core He flash in low-mass stars, except that the degeneracy is so strong that it can only be lifted when the temperature has reached about $10^{10}$ K. The ignition of carbon therefore causes the incineration of all material in the core of the white dwarf to Fe-peak elements (in nuclear statistical equilibrium). An explosive burning flame starts to propagate outwards, behind which material undergoes explosive nuclear burning. The composition of the ashes depends on the maximum temperature reached behind the flame, which decreases as the burning front crosses layers of lower and lower densities (although still degenerate). The composition is mainly $^{56}$Ni in the central parts, with progressively lighter elements (Ca, S, Si, etc) in more external layers. The total energy released by nuclear burning is of order $10^{51}$ erg, which is sufficient to overcome the binding energy of the white dwarf in the explosion. Therefore no stellar remnant is left.

The lightcurve of a Type Ia supernova is powered by the radioactive decay of the $^{56}$Ni formed in the explosion. The nickel mass is a substantial fraction of the mass of the white dwarf, $0.5 - 1.0\ M_\odot$, which is the main reason for the greater peak luminosities of SNe Ia compared to most core-collapse supernovae. About 50 days after maximum brightness, an exponential decay of the lightcurve occurs due to radioactive decay of $^{56}$Co into $^{56}$Fe.

In single stars of intermediate mass, the degenerate CO core cannot grow to the Chandrasekhar limit because mass loss quickly removes the envelope during the AGB phase (Ch. 11). Even if the Chandrasekhar limit were reached, the remaining H-rich envelope would cause a strong hydrogen signature in the supernova spectrum which is not seen in SNe Ia. Therefore it is commonly agreed upon that the CO white dwarfs that cause SN Ia explosions grow by accreting mass in a binary

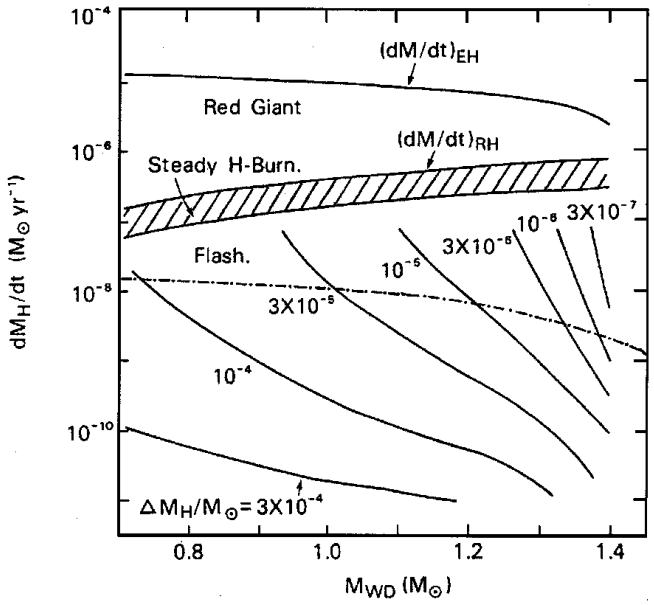


**Figure 13.4.** Critical mass transfer rates for hydrogen-accreting white dwarfs, as a function of the WD mass. Only for a small range of mass transfer rates (hatched area) can the material quietly burn on the WD surface, and thus lead to a growth of the WD mass towards the Chandrasekhar mass and a SN Ia explosion. (Figure from Kahabka & van den Heuvel 1997).

system. However, the exact mechanism by which this happens is still a matter of debate. Two types of progenitor scenarios are being discussed:

**The single degenerate scenario** In this scenario the white dwarf accretes H- or He-rich matter from a non-degenerate binary companion star: a main-sequence star, a red giant or a helium star (the stripped helium core of an initially more massive star). The difficulty is that steady burning of H and He, leading to growth of the mass of the white dwarf, is possible only for a narrow range of accretion rates (see Fig. 13.4). If accretion is too fast, a H-rich envelope is formed around the white dwarf (which would have an observable signature if the WD explodes). If accretion is too slow, the accreted matter burns in unstable flashes (*nova* outbursts) that throw off almost as much mass as has been accreted, such that the WD mass hardly grows. At present such models are too restrictive to explain the observed rate of SN Ia in galaxies.

**The double degenerate scenario** In this case the Chandrasekhar limit is reached by the merging of two CO white dwarfs in a close binary system. Such a close double WD can form as a result of strong mass and angular momentum loss during binary evolution (a process called *common envelope* evolution). Once a close double WD system is formed, angular momentum loss by gravitational waves can bring about the eventual merger of the system. Although at present no convincing evidence exists for a double WD binary with a total mass in excess of $M_{\rm Ch}$, the theoretical merger rate expected from binary evolution models appears sufficient to explain the observed SN Ia rate (note, however, that these models have large uncertainties). The main doubt about this scenario is whether the C-burning initiated by the WD merger leads to the required incineration and explosion of the merged white dwarf, or proceeds quiescently and results in a core collapse.

---

## Suggestions for further reading

See Chapter 28.4-6 of Maeder.

---

## Exercises

### 13.1 Energy budget of core-collapse supernovae

(a) Neutron stars have a radius of about 10 km. Use this to estimate the energy generated during a core collapse supernova (Hint: assume that before the collapse the core is like a white dwarf with mass $M_{\rm c} = M_{\rm Ch}$, where $M_{\rm Ch}$ is the Chandrasekhar mass, and that it suffers no significant mass loss after the collapse).

(b) The kinetic energy measured in the supernovae ejecta is about $E_{\rm kin} = 10^{51}$ erg. What is a typical velocity of the ejecta, if the original star was one of $10\,M_\odot$?

(c) The supernova shines with a luminosity of $2 \times 10^8\,L_\odot$ for about two months. Estimate the total energy in form of photons.

(d) Which particles carry away most of the energy of the supernova? Assuming an average energy of 5 MeV of those particles, how many of them are created by a supernova?

### 13.2 Neutrino luminosity by Si burning

Silicon burning forms iron out of silicon. Assume that 5 MeV of energy are liberated by creating one $^{56}$Fe nucleus from silicon, and that the final result of this burning is an iron core of about 2 $M_\odot$. Silicon burning only lasts about one day, as most of the liberated energy is converted into neutrinos (of about 5 MeV each).

(a) Compare the corresponding neutrino luminosity to that of Supernova 1987A, which can be well approximated by the calculations in Exercise 13.1.

(b) Now, knowing that this supernova was 50 kpc away, and that about 10 neutrinos were detected during one second: how close does the silicon burning star have to be, such that we can detect the neutrino emission?

### 13.3 Carbon ignition in a white dwarf

When a white dwarf approaches the Chandrasekhar mass, its central density exceeds $2 \times 10^9$ g/cm$^3$, carbon is ignited under degenerate conditions which will quickly burn the whole white dwarf to iron-group elements (mainly $^{56}$Ni). Compare the energy liberated by nuclear fusion to the gravitational binding energy of the white dwarf. What will be the outcome? (Use the masses of $^{12}$C, $^{16}$O and $^{56}$Ni nuclei in Table 6.1, and assume that the white dwarf is composed of equal mass fractions of $^{12}$C and $^{16}$O.)

# Contents